Fission fragment mass dependent prompt neutron emission investigation for resonance neutron induced fission of [235]U and for [252]Cf(SF).

F.-J. Hambsch[1], Sh. Zeynalov[1, 2], S. Oberstedt[1], I. Fabry[1].

[1] EC-JRC-Institute for Reference Materials and Measurements, Retieseweg 111, B-2440 Geel, Belgium
[2] Joint Institute for Nuclear Research, Joliot Curie 6, Dubna, Moscow region, Russia

Abstract

The prompt neutron emission in resonance neutron induced fission of [235]U and spontaneous fission of [252]Cf was investigated at GELINA using 8 large volume scintillation detectors from the DEMON collaboration. Pulse shape analysis and time-of-flight information of the neutron detector data was used to separate the prompt neutron emission from the γ-ray background from the fission process. The determination of the neutron spectrum and multiplicity is rather complicated due to the setup of the experiment. Different intermediate results are shown, however, the full data analysis is still ongoing.

Introduction

The resonance neutron induced fission of [235]U and [239]Pu was investigated intensively for decades because of its importance for nuclear power production at one hand and for the understanding of the fundamental aspects of the nuclear fission process at the other hand. Experimental investigations of prompt neutron distribution for resonance neutron induced fission carried out in the early 1970-ties for both uranium and plutonium detected small fluctuations of the prompt neutron multiplicities between resonances [1, 2]. The nature of these fluctuations is still not clearly understood and that fact stimulated more elaborated investigations. In the 1980-ties at IRMM fission fragment (FF) mass fluctuations were first observed in resonance neutron induced fission of [235]U [3] and in the late 1990-ties similar fluctuations were reported in Refs. [4, 5] for [235]U and [239]Pu. The average number of the fluctuations of prompt fission neutrons was correlated with the fluctuations of the fission fragment average TKE value. To get closer to the full understanding of the fluctuations, as a next step a more complete measurement should be envisaged to include the prompt neutron emission together with fission fragment information. This has now been started at IRMM.

Experimental setup

The experimental setup, consisting of 8 large volume (4 litre of NE213 liquid scintillator) neutron detectors from the DEMON collaboration and a double Frisch-grid back-to-back ionization chamber, was used in the measurements of $^{235}U(n_{res}, f)$ and $^{252}Cf(sf)$. Fig. 1 shows a schematical view of the experimental setup. The data acquisition electronics based on standard CAMAC modules was used for multi-parameter measurements including digitization of correlated fission fragments pulses, resonance neutron time-of-flight (TOF), prompt neutron TOF and prompt neutron pulse shape separation parameters. The data acquisition software was a modified version of the program used in the measurements reported in Ref. [4] to record list-mode data. Prompt neutron multiplicity data for the $^{235}U(n_{res}, f)$ reaction were evaluated using the $^{252}Cf(sf)$ reaction data, taken in identical measurement conditions (with the resonance neutron beam on).

0.85 M   0.85 M

DEMON modules 1-4

DEMON modules 5-8

NE213

NE213

Target

Neutron beam

NE213

NE213

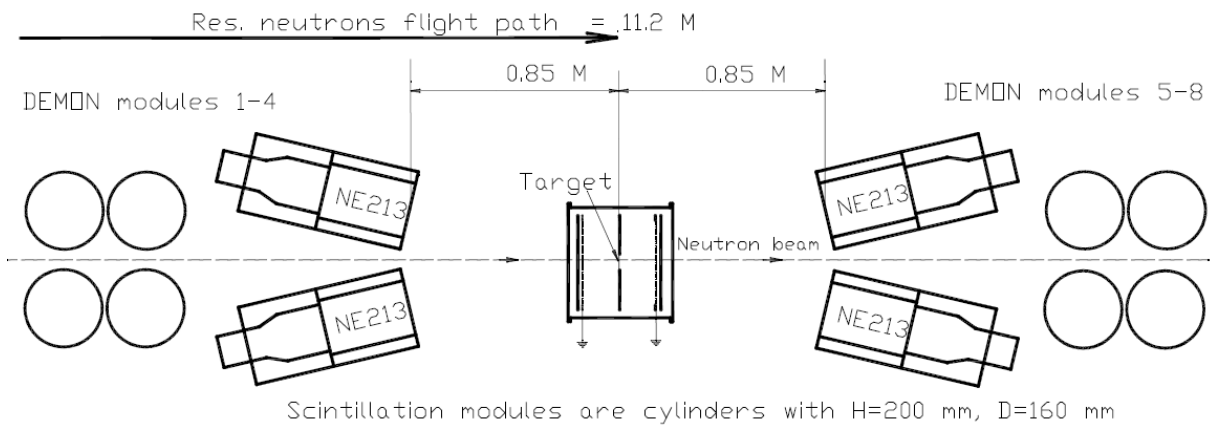Scintillation modules are cylinders with H=200 mm, D=160 mm

Fig. 1. Experimental setup.

Fission fragment mass and TKE measurements were carried out with a double channel waveform digitizer (WFD) having a sampling rate of 80 MHz and pulse height resolution of 10 bits. The information about FF kinetic energies and orientation with respect to the chamber axis was retrieved from the digitized anode current pulses. The neutrons were detected in coincidence with FF and were separated from the prompt gamma rays using a pulse shape discrimination technique.
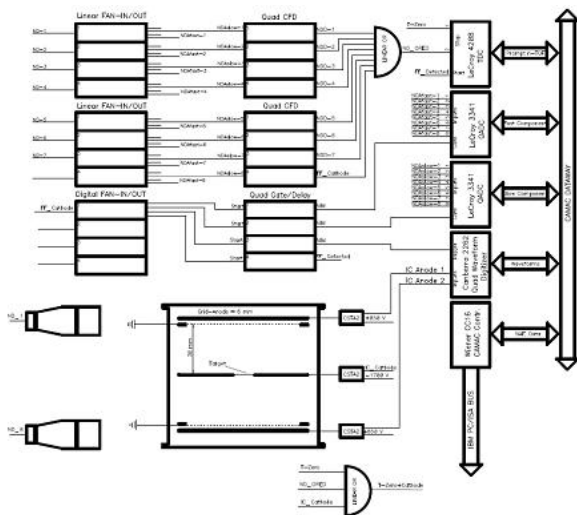
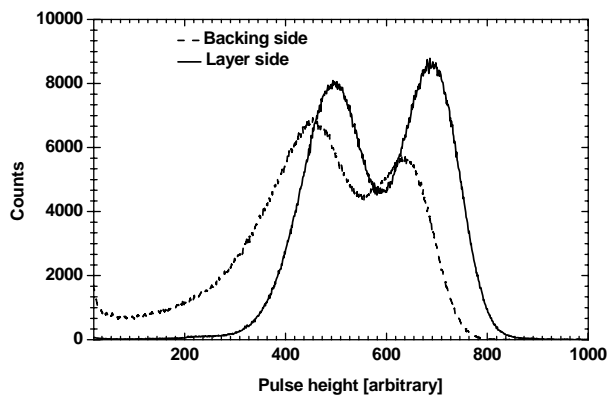Fig. 2. A schematical view of the data acquisition system.

Fig. 3. ^{252}Cf(sf) pulse height distribution obtained using digitization of the current pulses and digital filtering.

The block diagram of the electronics and the data acquisition system is presented in Fig. 2. The FF detection by the ionization chamber triggered the pulse processing chain consisting of a pair of WFD's, a time-to-digital converter (TDC) and a pair of current integrators (QDC). A coincidence of the common cathode signal and the logical sum (logical OR of ND signals) of the ND signals triggered the gate generators. A pair of gate generators controlled two QDCs having eight inputs each. The first QDC served to integrate the current of the eight NDs during 25 nsec (Fast component of the light output of the ND) and the other one was used to integrate the current of the NDs during 250 nsec (Total light output of the ND). The gate signals were arranged to coincide with the ND signals using specially adjusted delay lines. The TDC was brought to its initial state by every "T-Zero" signal from the

LINAC machine. When a FF signal was detected, its time of arrival was encoded by one of the 8 channels of the TDC, for the ND signal, if any of the eight NDs was detected, also the time of arrival was encoded by the second TDC channel. Approximately 200 μsec before the next "T-zero" signal the TDC internally generated an "end-of-window" signal initiating the data transfer to the PC. The real time data acquisition software after checking the content of the data record made the decision whether to store the data in the local memory or to discard them. The data were disregarded if a FF event was not detected.

A first measurement has been performed at a 10 m flight path at GELINA. At this distance, prompt fission neutron measurements are complicated due to various technical reasons, such as high neutron and gamma-ray background from the LINAC, the gamma-ray background from the investigated fission fragments, high gamma background from resonance neutron induced reactions on surrounding materials, and some other sources. These background problems became important because of the low geometrical efficiency of the available neutron detection system. To overcome these difficulties the experimental arrangement should be very carefully designed and well optimized.

Investigations of both analogue and digital pulse processing procedures of prompt fission neutron TOF measurements were carried out in order to improve the resolution of the TOF measurements. The results of that investigation are summarised in Ref. [6] where a procedure for TOF measurements was suggested that provides an optimal neutron-gamma separation. It was clearly demonstrated in Ref. [6] that the best accuracy of prompt neutron TOF measurement can be achieved in the prompt neutron energy range from ~350 KeV up to 20 MeV when the TOF and pulse height information from the NE213 based neutron detector are considered simultaneously.

Results

The pulse height distributions for both backing and layer sides of the ^{252}Cf(SF) target using a rectangular shaped filter implemented in the digital signal processing analysis are presented in Fig. 3. Based on these data and the necessary corrections for grid inefficiency, energy loss in target and backing and correction for prompt neutron emission the mass distributions could be generated as shown in Figs. 4, 5 for ^{252}Cf(SF) and ^{235}U(n,f). In both cases a good agreement with literature data was found. Fig. 6 shows the neutron time-of-flight spectrum with the resonance structure of ^{235}U(n,f). Although the distance to the neutron producing target is only about 10 m clearly resolved resonances are distinguishable.
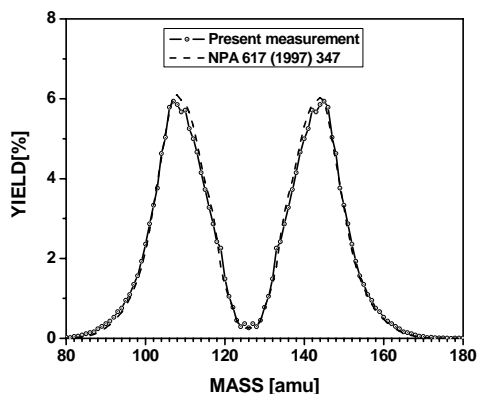

Fig. 4. Comparison of the measured mass distribution for ^{252}Cf(SF) with literature values.

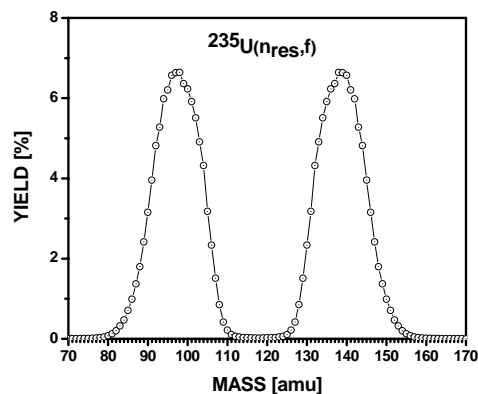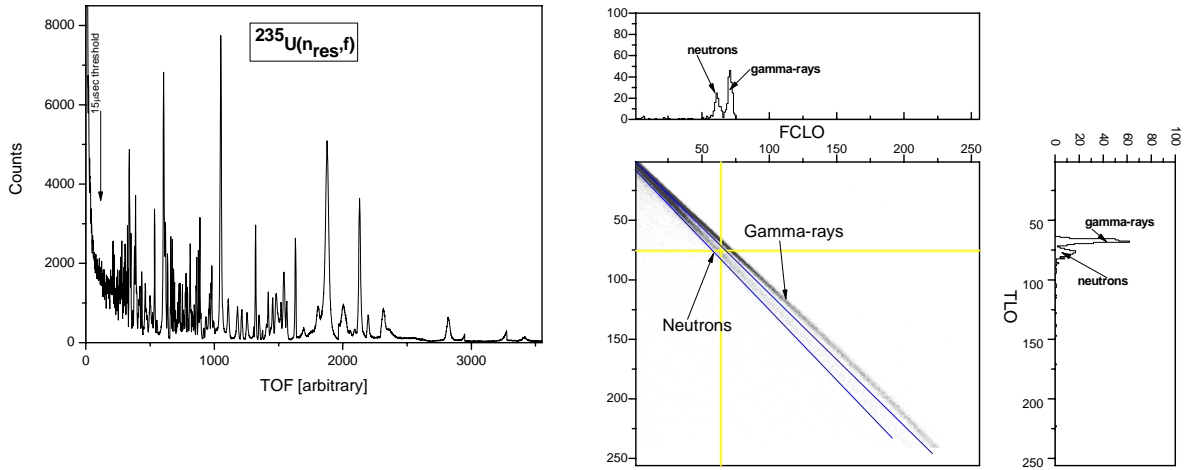Fig. 5. The measured mass distribution for ^{235}U(n,f) summed over the resonance region.

Fig. 6. Incident neutron time-of-flight distribution in the resonance region. Individual resonances are resolved.

Fig. 7. Pulse shape discrimination of the gamma-rays from the prompt fission neutrons.

A typical pulse shape analysis for the neutron detector signals relies on the difference between the slow and fast scintillation components. Fig. 7 illustrates the two-dimensional distribution plotted for the neutron detector pulses as FCLO (Fast Component Light Output - horizontal axis) versus TLO (Total Light Output - vertical axis). Such kinds of plots were used to separate the neutrons from the gamma-rays occupying different areas. The straight
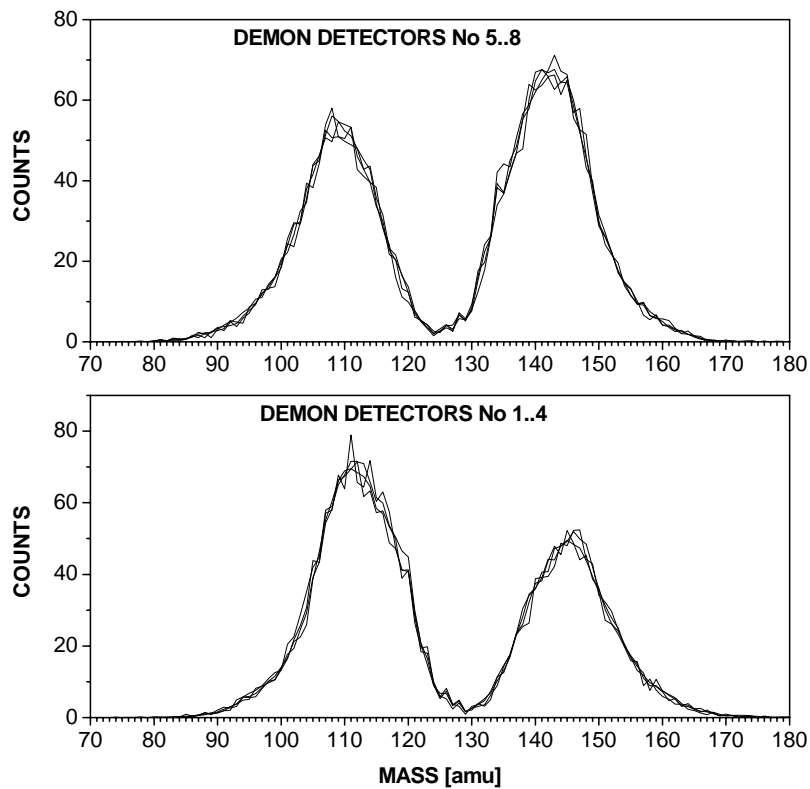

Fig. 8. Mass distribution plotted for the FF detected in coincidence with neutron detection in the different neutron detectors.

lines separating the neutron and gamma-ray distributions were drawn using the points in profiles, confining "the neutron" area shown on the right side (for the vertical profile) and on the upper plot (for the horizontal profile). After this pulse shape separation criterion was implemented the ND pulses having TOF values in the range corresponding to the neutron energies from 0.1 MeV to 30 MeV were assigned to the prompt fission neutrons. The FF mass distributions in coincidence with prompt fission neutrons are plotted in Fig. 8 for the forward hemisphere (DEMON detectors 5..8) and backward hemisphere (DEMON detectors 1..4). The distributions for different NDs were normalized to the same neutron detection efficiency values and their displacements were corrected for shifts caused by the different photomultiplier tubes used in the modules.

Individual prompt neutron TOF distributions (for each individual ND module) are presented in Fig. 9 along with integrated TOF distributions in forward and backward directions. The TOF distributions were measured with the TDC having 1 nsec resolution. The position of the peak caused by the prompt gamma-rays accompanied fission was used as reference point for the TOF measurements. Taking into account the distance between the ^{252}Cf target and the scintillator module having dimensions of $\varnothing 160 \times 200$ mm the average flight path was found to be FP = (0.85 ± 0.025) m.
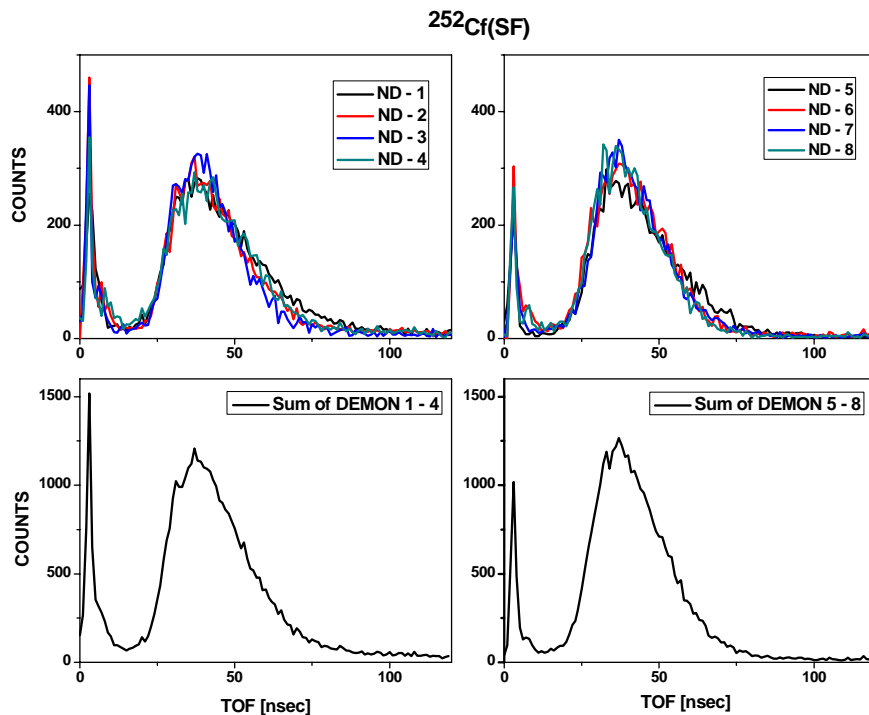

Fig. 9. TOF distribution for prompt fission neutrons from the ^{252}Cf(SF) for individual NDs in the forward (NDs 5-8) and the backward (NDs 1-4) hemispheres.
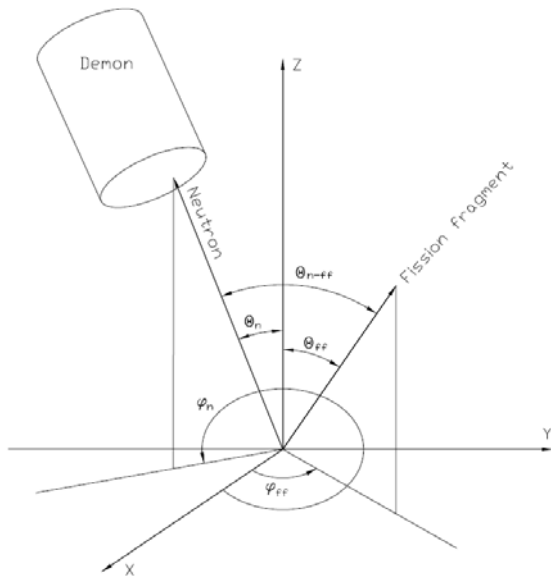
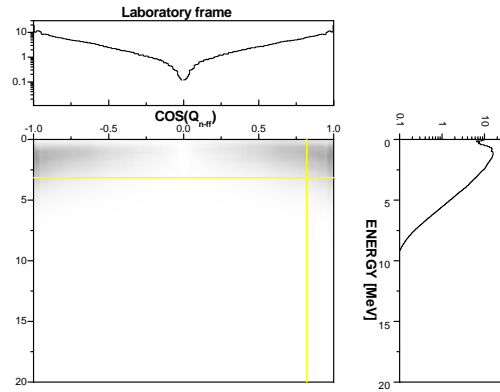Fig. 10. Setup of the DEMON detectors relative to the sample position.

Fig. 11. Cosine between FF and neutrons versus neutron kinetic energy in the laboratory frame.

The kinematics of neutron emission in the laboratory frame is illustrated in Fig. 10. The neutron emission was described by the unit vector *(cos(Θ_n)*cos(φ_n), cos(Θ_n)*sin(φ_n), sin(Θ_n))*, the FF was described by the unit vector *(cos(Θ_ff)*cos(φ_ff), cos(Θ_ff)*sin(φ_ff), sin(Θ_ff))*. The cosine of the angle between the neutron and the FF can then be found as:

$$\cos(\Theta_{n-ff}) = \sin(\Theta_{ff}) \times \sin(\Theta_n) \times \cos(\varphi_{ff} - \varphi_n) + \cos(\Theta_{ff}) \times \cos(\Theta_n) \qquad (1)$$

The vector *(cos(Θ_n)*cos(φ_n), cos(Θ_n)*sin(φ_n), sin(Θ_n))* is well defined for any of the 8 ND, the *cos(Θ_ff)* can be measured using the IC as was described above. The angle *φ_ff* can not be determined using the described experimental set-up meaning that it is folded in the experimental data. The solid angle for the neutron emission in the laboratory frame is given by:
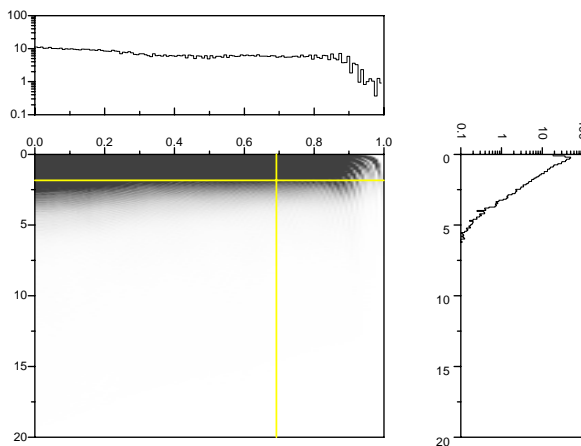

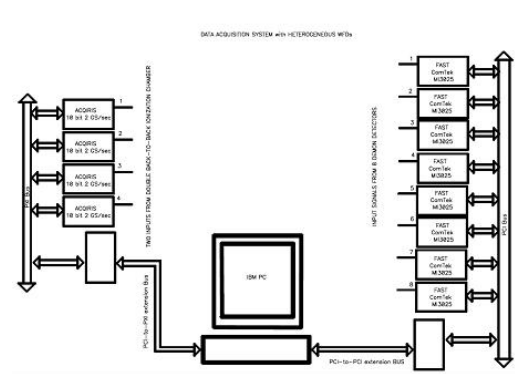Fig. 12. Cosine between FF and neutrons versus neutron kinetic energy in the centre-of-mass frame

Fig. 13. A schematical view of the fully digital data acquisition system.

$$dΩ_{lab} = -2 \times π \times d \cos(Θ_{n-ff}) = 2 \times π \times \sin(Θ_{n-ff}) \times dΘ_{n-ff} \quad (2)$$

In our data analysis procedure we considered the neutron emission kinematics in the ^{252}Cf(SF) reaction in the same way as it was done in Ref. [7]. Only FFs having COS($Θ_{ff}$) > 0.2 were taken into account in the analysis. The solid angle in the centre-of-mass frame can be found using equations (1-2) from Ref. [7]:

$$dΩ_{cm} = 2 \times π \times \frac{V_{lab}}{V_{cm}} \times \left[1 + \frac{(V_{lab} \times \cos(Θ_{n-ff}) - V_{F1}) \times V_{F1}}{V_{cm}^2}\right] \times \sin(Θ_{n-ff}) \times dΘ_{n-ff} \quad (3)$$

As neutron energy and angular distributions were folded in the measured data an unfolding procedure should be implemented in the data analysis. The unfolding of the present data was carried out using the following ideas. The TOF distribution was treated as the probability density function for the detected neutron. The same holds true for angular information unfolding. That is why both the energy and the angular distributions were normalised to unity as follows:

$$\int Φ(E)dE = 1, \quad \int_0^{4π} dΩ = 1. \quad (4)$$

Unfolded data plots for prompt neutron kinetic energy versus cosine of the angle between FF and neutron are given in Figs. 11 and 12 in the laboratory and centre-of-mass frames, respectively. The full data analysis is still in progress.

Finally a fully digital system to be used for the present type of measurements is under development. Fig. 13 gives a schematical view of the new data acquisition system consisting of a 4 channel, 2 GHz per channel, 10 bit Aqiris digitizer and 4 2 channel, 100 MHz per channel, 12 bit FASTCom digitizers connected via a high speed link to a PC running the acquisition software.

References

[1] J. Fréhaut, D. Shackleton in Proc., in Proc. 3rd Symp. Physics and Chemistry of Fission, IAEA Vienna, 1974, 201.
[2] R.E. Howe, T.W. Philips, and C.D. Bowman, Phys. Rev. C13 (1976) 195.
[3] F.-J. Hambsch, H.-H. Knitter, C. Budtz-Jørgensen, J.P. Theobald, Nucl. Phys. A491 (1989) 56.
[4] Sh.S. Zeinalov, M. Florek, W.I. Furman, V.A. Kriatchkov, Yu.S. Zamyatnin, Proc. VII Int. Seminar on Interaction of Neutrons with Nuclei (ISINN-7), Dubna, Russia, May 25-28, 1999, p.258.
[5] L. Demattè, F.-J. Hambsch, H. Bax, in: C. Wagemans, O. Serot, P. D'Oye IV", October 6-9, 1999, Habay-la-Neuve. World Scientific, Singapore, 2000, p. 135.
[6] Sh. Zeynalov, EC-JRC-IRMM Internal report GE/NP/07/2006/12/12.
[7] C. Budtz-Jørgensen and H.-H. Knitter, Nucl. Phys. A490 (1988) 307.